Probabilistic Optimization of a Continuum Mechanics Model to Predict Differential Stress-Induced Damage in Claystone

Esmaeel Bakhtiary, Hao Xu, Chloé Arson

School of Civil and Environmental Engineering,
Georgia Institute of Technology,
Atlanta, Georgia 30332, U.S.A.

Abstract

Phenomenological modeling of anisotropic damage in rock raises many fundamental thermodynamic and mechanical issues. In this paper, the maximum likelihood method is used to analyze the performance of the Differential Stress Induced Damage (DSID) model recently formulated by the authors [**?**]. The stress/strain relationship is a nonlinear function of parameters including unknown constants (i.e., damage constitutive parameters) and known variables (e.g., elastic parameters, controlled stress state). Logarithmic transformation, normalization and forward deletion are employed, in order to find the optimum number of constitutive parameters, as a trade off between accuracy and simplicity. For Eastern France claystone subject to deviatoric stress loading (e.g., triaxial and proportional compression loading), it is found that: (1) only one damage parameter ("a_2") is needed in the expression of the free energy to predict stress/strain curves; (2) a_2 controls the deviation of the current principal directions of stress to the principal directions of damage; (3) model parameters involved in the damage criterion can be related to a_2. As a result, a_2 is the only parameter needed to model differential-stress induced damage in Eastern France claystone. It is also shown that within the set of assumptions made in this study, the DSID model is not sensitive to the initial damage threshold C_0, except for $C_0 > 10^6$ Pa, a range of values in which only one constitutive parameter becomes insufficient to predict the stress/strain curves of damaged claystone. Coupling probabilistic calibration and optimization methods to numerical codes promises to allow adapting the complexity of anisotropic damage models to different rocks and stress paths.

Preprint submitted to International Journal of Rock Mechanics & Mining SciencesMay 28, 2014

Keywords: Rock Mechanics, Damage Mechanics, Thermodynamics, Maximum Likelihood Method, Model calibration, Performance assessment

1. Introduction

At present, 85% of the energy power consumed in the world is produced by fossil fuel combustion [**?** **?**], which has raised increasing interest in renewable energy technologies, non-conventional oil and gas reservoirs, and nuclear power. Innovative nuclear fuels and reactors depend on the economical and environmental impacts of waste management [**?**]. Disposals in mined geological formations are viewed as potential consolidated storage facilities before final disposition [**?**]. Rock damage is therefore a core issue in energy production (e.g., hydraulic fracturing [**?** **?** **?**], geothermal energy extraction [**?** **?** **?**]) , energy storage (e.g., Compressed Air Energy Storage [**?** **?** **?**]) and waste management (e.g., nuclear waste disposals [**?** **?** **?** **?** **?**], carbon capture [**?** **?** **?** **?**]). Continuum Damage Mechanics (CDM) provides an efficient framework to bridge failure plane scale with pore and crack scale. Damage is a thermodynamic variable used to: (1) represent crack initiation, propagation and coalescence in rock; and (2) model the subsequent changes of rock mechanical, physical and chemical properties at the scale of a Representative Elementary Volume (REV) [**?** **?**].

CDM-based models have an important practical interest for engineers, and are based on rigorous closed-form formulations. However, the difficulty to determine the magnitude of material parameters is overwhelming. The maximum likelihood method has been widely used in the past to find the optimum values of unknown parameters in probabilistic models. This method can also be employed to determine the standard error associated with a model, in order to assess the accuracy and reliability of this model. Also, it is possible to establish a procedure to remove unnecessary parameters or combine the ones which are correlated with each other. As a result, simpler models can be obtained, with fewer parameters. The maximum likelihood method also provides some insight on the relative importance of parameters in real physical problems. For instance, Ledesma et al. [**?**] used this method to find a constitutive model for soft biological tissues. Jung et al. used a Bayesian updating method (based on the maximum likelihood method) to find a constitutive law in a simplified unified compression model for soil deposits [**?**], and to improve soil classifications [**?**]. Medina-Cetina and Arson

[?] and Arson and Medina-Cetina [?] used the Bayesian paradigm to calibrate a damage mechanics model for rock, and to interpret the mathematical independence of the constitutive parameters. Boyce and Chamis [?] used both the maximum entropy principle and the maximum likelihood method to establish probabilistic constitutive relationships for cyclic material strength models. Gardoni et al. [? ?] used a total of 384 strand test specimens to study self-consolidated concrete exposed to various void, moisture, and chloride concentration conditions. Using experimental results and the maximum likelihood method, a probabilistic model was developed. Tsuchiya et al. [?] estimated the Weibull modulus of brittle materials using the maximum likelihood method. Instead of using a linear regression method, Huang et al. [?] employed the maximum likelihood method to predict concrete compressive strength using ultrasonic pulse velocity and rebound number. Trejo et al. [?] and Pillai et al. [?] identified and quantified important parameters influencing the corrosion and tension capacity of strands in post-tensioned bridges.

In the work presented in the following, the maximum likelihood method is used to analyze the performance of the Differential Stress Induced Damage (DSID) model recently formulated by the authors [?], with a particular focus on the stress/strain response of Eastern France claystone subjected to deviatoric stress loading. The main mineral and mechanical properties of the claystone under study are summarized in Section 2, along with the main constittive models proposed so far. Section 3 outlines the thermodynamic framework of the DSID model, and provides the state-of-the-art of the methods available to calibrate the related damage constitutive parameters. The proposed probabilistic model is presented in Section 4: known variables and unknown parameters are identified first, the implementation of the maximum likelihood method is explained then, and a probabilistic strategy is finally established for the use of the DSID model. Section 5 highlights the need for a parameter calibration, and methodically presents the optimization procedure used in this study. Section 6 discusses the significance of the results, and provides further performance assessment of the DSID model.

2. Overview of the Characterization and Modeling of Claystone

2.1. Mineral Composition and Physical Properties

Claystone is a mudrock - a class of fine grained siliciclastic sedimentary rocks. More than 50 percent of the composition of claystone is clay-sized

particles, less than 4μm in size. Clasystones contain quartz, feldspar, iron oxides, and carbonate minerals (in variable proportion, depending on the geological formation). In general, claystones tend to have low permeability but high mechanical strength. Clay minerals such as smectite and illite are very sensitive to the saturation degree, which can result in pronounced plastic deformation [**?**]. The behavior of claystone is more brittle when calcite content increases, and inversely becomes more ductile when the quantity of clay elements increases [**?**]. There is also a strong dependence of the mechanical behavior on the confining pressure, marked by a transition from a fragile towards a ductile behavior [**?**]. Table **??** summarizes the mineral and physical characteristics of claystones.

2.2. Experimental Characterization

Claystones are sedimentary rocks: they are structured in layers by the process of deposition. At the microscopic scale, anisotropy is manifested by the sliding of clay sheets and the twilling in a few large calcite grains - two phenomena which are related to the distribution of voids in the clay matrix. At the scale of the laboratory sample (Representative Elementary Volume, REV), claystone anisotropy can be seen during a hydrostatic compression loading (e.g., [**?**]): the response of the material to the applied loading exhibits different deformation in the axial and radial directions. In order to capture the resulting intrinsic anisotropy of claystone mechanical behavior, loading tests have to be performed in directions parallel and perpendicular to the bedding planes. Figure **??** shows examples of typical stress/strain curves obtained during triaxial compression tests, for various confining pressures. The plots (reported from [**?**]) highlight the non-linear response of claystone under deviatoric stress loading. It is worth noticing that non-linearities occur early during the loading path, which implies that when damage occurs, micro-cracks start propagating at low stress and low deformation.

2.3. Constitutive Models

Due to their favorable strength and permeability properties, Callovo-Oxfordian claystones are seen as a possible host rock for radioactive waste geological barriers. As such, claystones have been studied thoroughly by the French National Agency for Radioactive Waste Management (ANDRA). Constitutive models coupling plasticity or viscoplaticity to damage mechanics were proposed in [**?** **?** **?**]. The effect of the water content and structural

anisotropy on the mechanical properties of claystone was explained in [**?**]. An elastoplastic damage model was also formulated within the framework of poromechanics [**?**] in order to account for hydromechanical couplings in the prediction of the evolution of the Excavation Damaged Zone (EDZ) [**? ?**]. Thermal heating generates important volume changes and pore pressure variations, which significantly affect the hydraulic and mechanical behaviour of claystone [**?**]. A homogenization approach was proposed, in which the clay matrix was assumed to be a solid (described by a pressure sensitive plastic model) containing spherical micropores [**? ?**]. Continuum Damage Mechanics (CDM) models were also proposed in order to predict thermal, hydraulic, and mechanical crack propagation in unsaturated rock surrounding nuclear waste disposals [**? ? ? ?**]. The advantage of such CDM models (compared to phenomenological models coupling damage and plasticity) is that only one dissipation potential is required to close the formulation [**?**]. The DSID model used in the following is based on a general, unifying mathematical framework and requires few constitutive assumptions [**?**]. The number of model parameters needed is then reduced by probabilitistic calibration.

3. The D.S.I.D. Model: Theoretical Framework, Calibration Issues

3.1. Outline of the Differential Stress-Induced Damage (DSID) Model

In most anisotropic damage models proposed for geomaterials, the free energy of the solid skeleton is expressed in terms of deformation [**? ? ? ? ? ? ? ?**]. As a result, the energy release rate $\mathbf{Y}$ (also called damage driving force) that is work-conjugate to damage is also a function of deformation. In most rock mechanics problems of interest in engineering, the REV is subject to known conditions of stress - not deformation. That is the reason why the free energy potential used in the proposed anisotropic damage model is expressed in terms of stress (Gibbs free energy, G_s). Macroscopic deformation and stiffness evolve with the propagation of cracks due to "splitting effects" (i.e. Griffith cracks) and due to "crossing effects" (i.e. equivalent cracks linking wing shear micro-cracks [**?**]). In order to capture both of these dissipative phenomena, the damage criterion is expressed in terms of a damage driving force depending on the major principal stress. Because rock strength increases with confining pressure, the damage criterion is sought in the form of a function of stress difference, therefore the name of the model: Differential Stress-Induced Damage (DSID) model. To stay within the framework of linear elasticity in the absence of damage, the expression of the free energy

is sought in the form of a polynomial quadratic in stress ($\boldsymbol{\sigma}$) [**?** **?**]. The thermodynamic framework of the DSID model is summarized in Table **??**. Stress/strain relationships are derived from the expression of the free energy, which accounts for the damaged elastic deformation stored in the material and for the surface energy dissipated by residual crack opening. The damage criterion is similar to Drucker-Prager plastic yield function, but depends on the energy release rate instead of stress. A projection operator is used to distinguish tension and compression damage. The positivity of dissipation is ensured by introducing an *ad hoc* damage potential, which makes the damage flow rule non-associate. The irreversible deformation due to damage follows an associate flow rule, so as to ensure the co-axiality between crack opening vectors and the principal directions of damage-induced deformation. A more complete presentation and justification of the DSID model is available in [**?**].

3.2. Experimental Determination of the DSID Model Parameters

Damage models proposed for rock that are based on expressions of the free energy similar to the one adopted in the DSID model have a damage criterion and dissipation flow rules different from the ones used in the DSID model: the definition of the damage driving force is unique to the DSID model. Parameters a_1, a_2, a_3, a_4, C_0 and C_1 were calibrated by Halm and Dragon [**?**] and by Shao et al. [**?**]. However, none of the two papers contains calibrated values for the entire set of parameters (a_1, a_2, a_3, a_4, C_0, C_1). One may argue that the set of values for a_1, a_2, a_3, a_4 found in [**?**] may be combined with the set of values for C_0 and C_1 found in [**?**], since the two papers deal with the same rock material. However, the two studies are based on different experimental data, so the set of model parameters could be inconsistent, or contain redundant parameters.

Calibration methods are rarely proposed in damage rock mechanics: only Halm and Dragon [**?**] and Hayakawa and Murakami [**?**] provided mathematical measurement strategies for calibration, which were later followed by other authors [**?** **?**]. Halm and Dragon's method is based on an iterative process, which reduces its applicability to models that have a limited number of parameters. Hayakawa and Murakami proposed different strategies for different experimental tests. In both Halm and Dragon's and Hayakawa and Murakami's techniques, parameters are all determined from one type of experiment, which implies that the calibrated parameters may provide erroneous predictions for stress paths other than the ones tested. Therefore,

calibration methods employed so far are not sufficient to determine the DSID parameters relevant for claystone: a more comprehensive analysis is needed, based on datasets obtained for different types of experiments (i.e., stress paths), with a sufficient number of experiments for each stress path.

In rock mechanics, experimental tests are mainly the triaxial compression test, the uniaxial compression test, the uniaxial tension test and the Brazilian test. In the DSID model, the damage driving force and damage variable cannot be measured directly: they are back-calculated from constitutive parameters and other variables. Components of the damage tensor have to be derived first, which then allows determining the DSID model parameters. Constitutive parameters of the DSID models include the Young's modulus (E_0) and Poisson's ratio (ν_0) of the pristine (undamaged) rock, the four constitutive damage parameters (a_1, a_2, a_3 and a_4) involved in the expression of the free energy, the initial damage threshold C_0, the damage hardening parameter C_1, and a damage parameter α, related to rock dilatancy angle [**? ?**].

The probabilistic calibration of the DSID model needs to be based on a sufficient and consistent set of experimental data (i.e. on a large enough number of experiments performed on the same type of rock). In this paper, it is proposed to focus on the calibration of the damage parameters of the DSID model (a_1, a_2, a_3, a_4, C_0, C_1, α) for claystone, based on given stress-strain curves obtained during triaxial compression and proportional tests reported in [**? ? ?**]. The probabilistic calibration is therefore based on the same material and on similar deviatoric stress paths. Table **??** explains the experimental data used in this study.

4. Construction of a Probabilistic Model for Damage Mechanics

4.1. Definition of the known variables and unknown parameters

Reported stress/strain curves obtained from experiments are compared to predictions of strain made with the DSID model, for known states of stress, and for known elastic parameters. A probabilistic model for one component of the total strain can be written as:

$$\epsilon^{(i)}\left(\mathrm{x}, \mathrm{B}\right) = \gamma\left(\mathrm{x}, \beta\right) + s\xi \tag{1}$$

where $\epsilon^{(i)}\left(\mathrm{x}, \mathrm{B}\right)$ is the predicted total cumulated strain at increment (i). Selected explanatory functions $\gamma\left(\mathrm{x}, \beta\right)$ provide a way to relate the total strains'

component $\epsilon^{(i)}$ to loading measures and rock properties (e.g., stress tensor, elastic material parameters). x is a vector of basic variables, assumed to be known or measurable, and that do not need calibration, such as the stress tensor and the elastic material parameters. $\mathrm{B} = (\beta, s)$ is the vector of unknown model parameters, in which s is the standard deviation of the model error, and ξ is a normal random variable with zero mean and unit variance. In this particular study, $\beta = \{a_1, a_2, a_3, a_4, C_0, C_1, \alpha\}$ is the vector of unknown model parameters that can be optimized.

Two assumptions are made in assessing the total strain in Eq. **??**: (1) the *homoskedasticity assumption* (i.e., s is assumed to be a constant independent of x), and (2) the *normality assumption* (i.e., ξ is assumed to have a normal distribution). Usually, both assumptions can be satisfied by performing transformations to stabilize the variance of the quantities of interest [**?**]. In this paper, a natural logarithmic transformation of total strain is adopted, and after transformation, the model writes:

$$\ln\left\{\epsilon^{(i)}\left(\mathrm{x}, \mathrm{B}\right)\right\} = \ln\left\{\gamma\left(\mathrm{x}, \beta\right)\right\} + s\xi \tag{2}$$

Note that the model error is written in the same way in both equations **??** and **??**, to indicate the generality of the approach: predicted strain (or the logarithm of predicted strain) is the sum of an explanatory function (or the logarithm of this function), and a function of error.

4.2. Application of the Maximum Likelihood Method

The purpose of the probabilistic calibration is to optimize the estimation of the vector of unknown model parameters $\mathrm{B} = (\beta, s)$. Two types of error may arise when predicting the total strain with an estimator of $\mathrm{B} = (\beta, s)$ instead of the actual value of $\mathrm{B} = (\beta, s)$: *aleatory uncertainties* (known as inherent variability or randomness) and *epistemic uncertainties*. The former are those that are inherent in nature: they are not related to the way the data or the predictions are observed, and they are not influenced by the observer. This kind of uncertainty is accounted for in the variables x and partly in the error term ξ. The epistemic uncertainties are those that are due to a lack of knowledge of processes, a deliberate choice to simplify models, or due to the finite size of experimental observation samples or to errors in measuring observations. This kind of uncertainty is present in the model parameters B and partly in the error term ξ. The fundamental difference between the two types of uncertainties is that, whereas aleatory uncertainties are irreducible,

epistemic uncertainties are reducible (e.g., by improving models, using more accurate measurements or collecting additional samples [**?**]).

$\hat{\mathrm{B}}$ is said to be an unbiased estimator of B if the expected value of $\hat{\mathrm{B}}$ is equal to B, i.e., if the mean of the probability distribution of $\hat{\mathrm{B}}$ is equal to B. One of the best methods to obtain a point estimator of a parameter is the method of Maximum Likelihood [**?** **?** **?**]. As the name implies, the estimation of B is based on the value of $\hat{\mathrm{B}}$ that maximizes the likelihood function, which is defined herein by using experimental data. Data points (noted $\epsilon_{\mathrm{exp}}^{(i)}$ to refer to experimental data) used as reference observation data are points of stress/strain curves collected from the literature (Tab. **??**). The vector of unknown model parameters is estimated ($\mathring{\mathrm{B}} = \{\mathring{a}_1, \mathring{a}_2, \mathring{a}_3, \mathring{a}_4, \mathring{C}_0, \mathring{C}_1, \mathring{\alpha}, \mathring{s}\}$), which allows computing the total strain $\mathring{\epsilon}^{(i)}$ using Eq. **??**: this provides a strain prediction with a certain error.

As discussed earlier, after performing the natural logarithmic transformation, the model error ξ is assumed to have a normal distribution. Therefore, using the well known Gaussian distribution, the probability distribution corresponding to $\mathring{\mathrm{B}}$ is written as:

$$P(\mathring{\mathrm{B}}) = \frac{1}{\mathring{s}\sqrt{2\pi}} e^{-\left(\epsilon_{\mathrm{exp}}^{(i)} - \mathring{\epsilon}^{(i)}\right)^2 / \left(2\mathring{s}^2\right)} \tag{3}$$

The above equation is the probability function for one point on the experimental stress-strain curve. Usually, not only several experiments are used for calibration, but also, several points of the stress-strain curve are read and used as observation data, for each experiment. Therefore, the likelihood function for a set of n independent experimental observations is written as:

$$L(\mathring{\mathrm{B}}) = \prod_{j=1}^{n} \frac{1}{\mathring{s}\sqrt{2\pi}} e^{-\left(\epsilon_{\mathrm{exp}_j}^{(i)} - \mathring{\epsilon}_j^{(i)}\right)^2 / \left(2\mathring{s}^2\right)} \tag{4}$$

For practical reasons in computer programs, the natural logarithm of the likelihood function is determined:

$$\ln\left\{L(\mathring{\beta})\right\} = \sum_{j=1}^{n} \ln\left\{\frac{1}{\mathring{s}\sqrt{2\pi}} e^{-\left(\epsilon_{\mathrm{exp}_j}^{(i)} - \mathring{\epsilon}_j^{(i)}\right)^2 / \left(2\mathring{s}^2\right)}\right\} \tag{5}$$

Because the logarithm is a one-to-one function, Eq. **??** above allows determining the likelihood function defined in Eq. **??**. The value of the likelihood function is obtained for the assumed set of values $\mathring{\mathrm{B}}$ taken by the unknown

model parameters. To obtain the optimum representative values of the components of the vector of unknown model parameters B, simulations were performed by using the built-in function *fmincon* in MATLAB: the likelihood function was computed for several hundreds of sets of values assigned to the vector of unknown model parameters. The set of parameters that maximizes the likelihood function is retained to estimate the vector of unknown model parameters B. Other statistical properties, such as the standard deviation and the correlation coefficient matrix, can also be determined.

4.3. DSID Model Calibration: Probabilistic Strategy

As mentioned earlier, the aim of this study is to optimize the set of model parameters $\beta = \{a_1, a_2, a_3, a_4, C_0, C_1, \alpha\}$ for claystone, based on the observation data set presented in Tab. **??**. The one-point estimator is based on the prediction of the total, cumulated strain $\epsilon^{(i)}(\mathrm{x}, \mathrm{B})$, from the knowledge of stress. From Tab **??**, we have: $\epsilon^{(i)} = \epsilon^{E\,(i)} + \epsilon^{id\,(i)}$. Strain estimation thus depends on the estimation of elastic parameters (to get the purely elastic part of $\epsilon^{E\,(i)}$), damage (to get the damage-induced part of $\epsilon^{E\,(i)}$), and irreversible deformation $\epsilon^{id\,(i)}$. The undamaged elastic parameters E_0 and ν_0 affect the elastic deformation energy that can be stored in the material before damage occurrence, which affects the total deformation during damage propagation. Therefore, the undamaged elastic parameters affect damage evolution, but indirectly. This study focuses on the brittle deformation regime, and to simplify the computations, the undamaged elastic parameters were not calibrated by the maximum likelihood method: instead, E_0 and ν_0 were taken equal to the values fitted on the experimental stress/strain curves used as reference data, as recommended by the authors [**?** **?** **?**]. The estimation of both $\epsilon^{E\,(i)}$ and $\epsilon^{id\,(i)}$ requires the computation of the damage variable $\mathbf{\Omega}$ at the point of observation (more details on the incremental constitutive laws of the DSID model are available in [**?**]). However, $\mathbf{\Omega}$ cannot be obtained directly from the stress/strain curves used for the reference observation data. Fortunately, it is possible to relate $\mathbf{\Omega}$ to measurable parameters and a set of unknown constants. Cumulated damage is the sum of all damage increments from "time 0" to "current time" (i.e. to observation point (i)):

$$\mathbf{\Omega}^{(i)} = \sum_{k=1}^{i} \dot{\mathbf{\Omega}}^{(k)} = \sum_{k=1}^{i} \dot{\lambda_d}^{(k)} \left(\frac{\partial g_d}{\partial \boldsymbol{\sigma}} \right)^{(k)} \tag{6}$$

Using the chain rule, the derivative $\frac{\partial g_d}{\partial \boldsymbol{\sigma}}$ in the right of Eq. **??** can be expressed with unknown model parameters a_i and the known variable $\boldsymbol{\sigma}$:

$$\frac{\partial g_d}{\partial \boldsymbol{\sigma}} = \frac{\partial g_d}{\partial \mathbf{Y}} : \frac{\partial \mathbf{Y}}{\partial \boldsymbol{\sigma}} \tag{7}$$

$$\frac{\partial g_d}{\partial \mathbf{Y}} = \frac{(\mathbb{P}_2 : \mathbf{Y}) : \mathbb{P}_2}{\sqrt{2(\mathbb{P}_2 : \mathbf{Y}) : (\mathbb{P}_2 : \mathbf{Y})}} \tag{8}$$

$$\frac{\partial \mathbf{Y}}{\partial \boldsymbol{\sigma}} = 2a_1(Tr\boldsymbol{\sigma})\mathbb{I} \otimes \mathbb{I} + a_2(\mathbb{I} \cdot \boldsymbol{\sigma} + \boldsymbol{\sigma} \cdot \mathbb{I}) + a_3[\boldsymbol{\sigma} \otimes \mathbb{I} + (Tr\boldsymbol{\sigma})\mathbb{I}] + 2a_4\,\mathbb{I} \otimes \boldsymbol{\sigma} \tag{9}$$

Where $\mathbb{I}$ is the symmetric fourth-order identity tensor:

$$\mathbb{I}_{ijkl} = \frac{1}{2}(\delta_{ik}\delta_{jl} + \delta_{il}\delta_{jk}) \tag{10}$$

In which $\boldsymbol{\delta}$ is the second-order identity tensor. The Lagrangian multiplier $\dot{\lambda}_d$ in the right of Eq. **??** is obtained from the consistency condition:

$$\dot{\lambda}_d = \frac{\dot{f}_d - \frac{\partial f_d}{\partial \mathbf{Y}} : \dot{\mathbf{Y}}}{\frac{\partial f_d}{\partial \boldsymbol{\Omega}} : \frac{\partial g_d}{\partial \mathbf{Y}}} \tag{11}$$

The derivatives $\frac{\partial f_d}{\partial \mathbf{Y}}$ and $\frac{\partial f_d}{\partial \boldsymbol{\Omega}}$ write:

$$\frac{\partial f_d}{\partial \mathbf{Y}} = \frac{\left[\mathbb{P}_1 : \mathbf{Y} - \frac{1}{3}\left(\boldsymbol{\delta} : \mathbb{P}_1 : \mathbf{Y}\right)\boldsymbol{\delta}\right] : \left[\mathbb{P}_1 - \frac{1}{3}\boldsymbol{\delta} \otimes (\boldsymbol{\delta} : \mathbb{P}_1)\right]}{\sqrt{2\left[\mathbb{P}_1 : \mathbf{Y} - \frac{1}{3}\left(\boldsymbol{\delta} : \mathbb{P}_1 : \mathbf{Y}\right)\boldsymbol{\delta}\right]\left[\mathbb{P}_1 : \mathbf{Y} - \frac{1}{3}(\boldsymbol{\delta} : \mathbb{P}_1 : \mathbf{Y})\boldsymbol{\delta}\right]}} - \alpha\boldsymbol{\delta} : \mathbb{P}_1 \tag{12}$$

$$\frac{\partial f_d}{\partial \boldsymbol{\Omega}} = -C_1\boldsymbol{\delta} \tag{13}$$

The same strategy can be used for irreversible strain:

$$\boldsymbol{\epsilon}^{id(k)} = \sum_{k=1}^{i} \dot{\boldsymbol{\epsilon}}^{id(k)} = \sum_{k=1}^{i} \dot{\lambda}_d^{\,(k)} \left(\frac{\partial f_d}{\partial \boldsymbol{\sigma}}\right)^{(k)} \tag{14}$$

As a result, the damage and irreversible strain cumulated at the point of observation can be determined from the known variable $\boldsymbol{\sigma}$ and the vector of unknown parameters $\beta = \{a_1, a_2, a_3, a_4, C_0, C_1, \alpha\}$, which makes it possible to make a prediction of the cumulated total strain from the DSID model for given states of stress. Therefore, it is possible to use a probabilistic approach to determine the statistical properties of all unknown parameters. Corresponding analyzes are provided in the next section.

5. Probabilistic Optimization of the DSID Model for Claystone under Deviatoric Stress Loading

5.1. Probabilistic Calibration of the DSID Model

The probabilistic model explained above is based on the iterative maximization of a likelihood function, in which the algorithm needs to be initiated with estimates of the unknown parameters. By definition, unknown parameters are not available in the literature. In the following analysis, the vector of unknown parameters is initialized with damage parameters found in the literature for granite: a_1, a_2, a_3 and a_4 are taken from the work by Shao et al. [**?**] for Lac du Bonnet granite; C_0 and C_1 are taken from the work of Halm and Dragon [**?**] for Vienne granite. The optimization method employed in this paper assumes that the unknown parameters can take any value, and the final result is independent of the initialization. However, a proper initialization helps to converge faster to the optimized results. The initial set of values for the components of the vector of unknown parameters β is presented in Table **??**.

From the high departure from the 1:1 line in Figure **??**a., it can be seen that the stress/strain curves predicted with the equations derived in Subsection **??** and the set of parameters tabulated in Table **??** do not match the experimental stress/strain curves used as reference data (Table **??**). Moreover, the standard deviation of the model increases for the larger values of strain. Using a natural logarithmic transformation (Eq. **??**) allows stabilizing the standard deviation, but does not improve the performance of the model (Figure **??**b.). Therefore, a rigorous calibration is needed to determine the set of unknown damage parameters $\beta = \{a_1, a_2, a_3, a_4, C_0, C_1, \alpha\}$.

In the process of maximization of the likelihood function, it was found that model performance is not sensitive to the initial damage threshold C_0 (this observation is confirmed in Subsection **??**, Figure **??**). Claystone is indeed a very brittle material, in which cracks develop early on during triaxial compression and proportional tests (Figure **??**). Once damage is initiated, the stress/strain curve is mostly influenced by the damage hardening parameter C_1. For high levels of damage, important irreversible deformation is expected: this behavior trend is herein referred to as "ductile deformation regime". To simplify the optimization process, the value of C_0 was fixed to a low value ($C_0 = 1.1 \times 10^5$ Pa, as reported in Table **??**), which made it possible to predict damage even at low deformation and stay in the brittle deformation regime - the focus of this study. Table **??** summarizes the values of the

remaining constitutive damage parameters $\{a_1, a_2, a_3, a_4, C_1, \alpha\}$, optimized by the maximum likelihood method. A comparison between results obtained using these values against experimental data are presented in Fig. **??**b. and Fig. **??**c. in normal and logarithmic scales, respectively. As it can be seen in these figures, predictions are noticeably improved after optimization, and the standard deviation in logarithmic scale remains constant for different values of strain. The standard deviation for the model is equal to 0.29. The standard deviation s for the model after logarithmic transformation is approximately equal to the Coefficient Of Variation (C.O.V in Table **??**) of the model before logarithmic transformation [**?**]. The Coefficient Of Variation (C.O.V in Table **??**), defined as:

$$C.O.V = SD/\mu \tag{15}$$

provides an indication on model uncertainty associated to a specific constitutive parameter. The C.O.V. is representative of the non-linearities of the DSID model, of the uncertainties involved in the prediction of the mechanical behavior of rock (which are natural materials), and of the measurement errors.

5.2. Probabilistic Optimization of the DSID Model: Removing Parameters

Deviatoric stress loading (e.g., triaxial compression tests, proportional loading tests), is a representative state of stress for many rock engineering applications. For instance, the rock mass undergoes differences of principal stress during the excavation of tunnels and during the pressurization of well bores. Therefore it is interesting to know whether the DSID model could be simplified for cases where damage is expected to occur due to deviatoric stress. In the following, it is proposed to assess the performance of the DSID model for the prediction of compression-induced damage, with a reduced number of constitutive parameters. Because the damage function is necessary to predict the occurrence of damage itself, related parameters C_0, C_1 and α are maintained in the model formulation. Probabilistic optimization is focused on parameters a_1, a_2, a_3 and a_4, involved in the expression of the free energy of the damaged rock (Table **??**). It is noteworthy that the polynomial used in the DSID model is similar to the one used by Shao et al. [**?**], while Halm and Dragon [**?**] used only two constitutive parameters. Shao et al. [**?**] observed experimentally that the damage model derived with four parameters was not sensitive to a_1, and therefore assumed $a_1 = 0$.

The objective of the following probabilistic optimization is to justify the form of the polynomial used in the free energy of damaged claystone from a mathematical stand point, for differential stress loading. The calibration results summarized in Table **??** indicate that: (1) a_4 has the largest C.O.V.; (2) a_4 has the minimum mean value. The first statement (1) implies that the DSID model is less sensitive to a_4 than to the other constitutive parameters. The second observation (2) supports this conclusion, since for a given state of stress, the order of magnitude of the monomials present in the expression of the free energy is controlled by the absolute value of the coefficient a_i multiplying them. The Maximum Likelihood Method is used to optimize the calibration of the set of parameters $\beta = \{a_1, a_2, a_3, C_0, C_1, \alpha\}$, i.e. to optimize the calibration of the DSID parameters when a_4 is removed from the formulation (i.e., when $a_4 = 0$). Results are presented in Table **??**.

Interestingly, the model standard deviation does not change after removal of the a_4 parameter: this means that for the stress path and material under study, a_4 does not contribute significantly to stress/strain prediction, and that a_4 (and its associated explanatory function) can be safely removed from the model formulation. The comparison between model predictions (without a_4) and experimental observations (Fig. **??**e. and Fig. **??**f.) confirm that model performance is not sensitive to a_4. By following the same procedure, parameters a_1 and a_3 are successively removed from the model formulation. Probabilistic results are presented in Table **??** and Table **??**, respectively. Comparisons between the predictions with a reduced number of model parameters and experimental observations show that neither a_1 (Fig. **??**g. and Fig. **??**h.) or a_3 (Fig. **??**c. and Fig. **??**d.) significantly affects the performance of the DSID model. Moreover, predictions obtained with a_2 only (Fig. **??**c. and Fig. **??**d.) are not significantly different from the ones obtained with the four constitutive parameters (Fig. **??**c. and Fig. **??**d). The performance of the model was assessed for other choices of single-parameter based formulations (i.e. a_1, a_3 or a_4 only): results confirm that a_2 is the only constitutive parameter needed to predict differential stress-induced damage in Eastern France claystone (Fig. **??**).

5.3. Probabilistic Optimization of the DSID Model: Combining Parameters

The correlation coefficient matrix for the remaining variables is shown in Table **??**. If the absolute value of the correlation coefficient between two variables (β_i and β_j) is close to one, the two variables have high correlation and may be combined using the following equation obtained from statistical

relations [**?** **?**]:

$$\hat{\beta}_i = \mu_{\beta_i} + \rho_{\beta_i\beta_j} \frac{SD_{\beta_i}}{SD_{\beta_j}} \left(\beta_j - \mu_{\beta_j}\right) \tag{16}$$

where μ_{β_i} (resp. μ_{β_j}) is the mean value of β_i (resp. β_j); $\rho_{\beta_i\beta_j}$ is the correlation coefficient between β_i and β_j; SD_{β_i} (resp. SD_{β_j}) is the standard deviation of β_i (resp. β_j); and $\hat{\beta}_i$ is the new estimate for β_i. According to Table **??**, the correlation coefficient between all variables is almost one. This means these variables are highly correlated with each other, which allows using Eq. **??** to combine parameters and reduce the number of independent model parameters in the formulation of the DSID model.

By substituting the values from Table **??** into Eq. **??**, the new estimates of C_1 and α can be written as functions of a_2:

$$\hat{C}_1 = 64.34 \times 10^6 + \frac{6.30 \times 10^6}{35.80 \times 10^{-11}} \left(a_2 - 704.94 \times 10^{-11}\right) \tag{17}$$

$$\hat{\alpha} = 3.29 \times 10^{-1} + \frac{0.26 \times 10^{-1}}{35.80 \times 10^{-11}} \left(a_2 - 704.94 \times 10^{-11}\right) \tag{18}$$

According to the preceding probabilistic optimization, the free energy of damaged claystone can be written as:

$$G_s(\boldsymbol{\sigma}, \boldsymbol{\Omega}) = \frac{1}{2}\boldsymbol{\sigma} : \mathbb{S}_0 : \boldsymbol{\sigma} + a_2 \,\mathrm{Tr}(\boldsymbol{\sigma} \cdot \boldsymbol{\sigma} \cdot \boldsymbol{\Omega}) \tag{19}$$

and the damage function writes:

$$f_d = \sqrt{J^*} - \hat{\alpha} I^* - C_0 - \hat{C}_1 \mathrm{Tr}\boldsymbol{\Omega} \tag{20}$$

in which C_1 and α are functions of a_2. Optimized values of a_2, C_1 and α, obtained by using the combinations above in the explanatory functions used in the maximum likelihood method, are provided in Table **??**.

6. Discussion

6.1. Physical Interpretation of the Model Optimization

The main finding of the preceding probabilistic analysis is that only two damage parameters are needed to predict damaged stress/strain curves of claystone subjected to deviatoric stress loading: C_0 and a_2. As mentioned earlier, the DSID model is not sensitive to C_0 in the brittle deformation

regime: it may be concluded that the only constitutive parameter needed to predict differential stress-induced damage in claystone is a_2, the coefficient multiplying the monomial $\mathrm{Tr}(\boldsymbol{\sigma} \cdot \boldsymbol{\sigma} \cdot \boldsymbol{\Omega})$ in the expression of the damaged free energy. The optimized formulation of the DSID model obtained after applying the maximum likelihood method is therefore much simpler than the one dictated by elasticity and thermodynamic principles, in Table **??**. The most general formulation of the DSID model needs however to be used as is, when no information is available on the type of rock material tested or stress path expected.

In triaxial compression and proportional tests, damage is driven by a deviatoric stress (in compression). By design, the DSID model captures anisotropic damage induced by differential stress. As a result, it is expected that explanatory functions depending on stress, differences of principal stresses in particular, should be the most affected by the stress path. Table **??** summarizes the relation of each a_i parameter to the free energy G_s, the total elastic deformation $\boldsymbol{\epsilon}^E$ and the damage driving force $\mathbf{Y}$. In the expression of the free energy, every a_i multiplies a trace of stress, damage or products of stress and damage. Therefore it is impossible to conclude on the relative importance of the constitutive parameters for the prediction of anisotropic damage induced by stress difference.

In the expression of total elastic strain, a_1 and a_3 multiply traces. Although the term in a_3 allows quantifying the deviation of stress from the principal directions of damage (i.e. from the "past" principal directions of stress), the relation to the anisotropic stress path is expected to be better captured by the terms in a_2 and a_4, which indeed contain a non-volumetric term of stress. In the expression of the damage driving force, only a_2 and a_3 multiply a non-volumetric stress. Hence, a_2 influences stress-induced damage and the subsequent anisotropy of both the elastic deformation and the damage driving force. Conceptually, it could be expected that a_2 would play the most important role in the damage model for the tests.

However, the order of magnitude of constitutive parameters is also critical in the analysis. From Table **??**, we have:

$$|a_4| < |a_1| < |a_3| < |a_2| \tag{21}$$

a_2 is two orders of magnitude larger than a_3, which is one order of magnitude larger than a_1 and a_4, a_1 being slightly larger than a_4. From this analysis, it can be recommended to simplify the DSID model by removing a_4 first, then

a_1, and finally a_3. a_2 turns out to be again the most significant parameter in the model. All of these analyses concur with the conclusions raised in the probabilistic optimization of the damage model.

6.2. Probabilistic Assessment of the Optimized DSID Model

The model optimization explained in Subsection **??** assumes that C_0 does not play a significant role on the evolution of damage, since cracking is expected to occur for low stress and low deformation in claystone. In order to check this assumption, the influence of parameter C_0 on the performance of the optimized damage model is assessed, after removing and combining parameters (Eq. **??**, **??**, **??**, **??**). Values of C_0 are varied between 0 and 10^7 Pa. Fig. **??** shows that model predictions are not affected by the initial damage threshold when $0 < C_0 < 10^5$ Pa. For $C_0 > 10^6$ Pa, the optimized damage model obtained previously tends to underestimate the total strain. This could be expected, since higher values of C_0 "delay" the occurrence of damage until higher stress differences are reached in the sample. Therefore, increasing the value of C_0 tends to under-estimate damage and the related damage-induced deformation components, which results in under-estimated total deformation. Therefore, it is recommended to use the optimized DSID model (based on a_2 only) for initial damage thresholds between 0 and $10^6\,Pa$.

The probabilistic calibration presented above is based on the optimization of the estimation of axial strain only. In order to properly assess the model performance, both axial (ϵ_{11}) and lateral (ϵ_{33}) strains predicted by the calibrated and optimized DSID model were compared to experimental stress/strain curves, in Fig. **??** and **??**. It appears that after simplification and calibration, the DSID model does not perform equally well for all the tests used as reference data. In summary, the results of tests 5, 9, 10, 12, 13 and 15 provide close prediction for vertical strains (Fig. **??**, **??**, **??**, **??**, **??** and **??**); while the simulations of tests 3, 4 ,11, 13, 15, and 16 show good match for lateral strains (Fig. **??**, **??**, **??**, **??**, **??** and **??**). The main reason for these differences is that the model was optimized on the basis of the entire experimental dataset, and the plots in Fig. **??** and **??** only show the results for one test at a time, which may deviate from the average response measured from all the reference tests.

Experimentally, it is observed that claystones generally do not dilate significantly upon deviatoric loading: the volumetric deformation are compressive. However, the important increase of radial strains at higher deviatoric

stress results in less compressive volumetric strains. In porportional tests, experimental measures indicate that lateral strains are almost zero, especially at low stress. Some of the predicted stress/strain curves underestimate radial strains, which tend to decrease upon deviatoric compression (Fig. **??** and **??**). Based on the simulation results obtained, it is noted that DSID predictions generally underestimate lateral strains for the higher deviatoric stress levels: the model does not capture the degradation of compressive volumetric strains. Moreover, it can be concluded that stress path affects the model calibration results.

7. Conclusion

Phenomenological modeling of anisotropic damage in rock raises many thermodynamic issues (e.g. ensuring the positivity of dissipation) and mechanical challenges (e.g. differentiating between tension and compression strength, accounting for the presence of frictional closed cracks). Moreover, rigorous calibration methods are missing: the rare procedures explaining the determination of damage model parameters from rock mechanics tests are usually limited to one stress path, and supported by a low number of physical experiments. In some models, it is even impossible to use direct measurements of stress and strain only, because any additional datapoint brings an additional unknown (the damage variable) in the set of equations to solve: an iterative procedure has to be followed in order to fit predicted sress/strain curves to experimental data.

In this paper, the maximum likelihood method is used to analyze the performance of the Differential Stress Induced Damage (DSID) model recently formulated by the authors, in order to predict the stress/strain response of claystone subjected to triaxial compression tests and proportional tests. The forward deletion approach is employed to find the optimum number of constitutive parameters as a trade off between accuracy and simplicity. It is found that: (1) only one damage parameter ("a_2") is needed in the expression of the free energy to predict stress/strain curves; (2) a_2 controls the deviation of the current principal directions of stress to the principal directions of damage (which are co-axial with the cumulated deviatoric stress); (3) model parameters involved in the damage criterion cannot be removed from the simulation, but can be related to a_2. As a result, the DSID model can

be simplified when used for claystone under triaxial compression tests and proportional tests: the model can be formulated with only one unknown a_2, which can be viewed as the only parameter needed to model differential-stress induced damage in Eastern France claystone.

To simplify the computations, the undamaged elastic parameters E_0 and ν_0 were taken equal to the values fitted on the experimental stress/strain curves used as reference data. Rigorously speaking, E_0 and ν_0 are expected to vary in a specific range of values. But for low levels of stress difference, claystone is a very brittle rock, so that both elastic parameters and the initial damage threshold (C_0) do not significantly affect the stress/strain curve. For higher levels of stress difference however, the DSID model is expected to be sensitive to C_0. The present study focuses on the brittle deformation regime of claystone, and as a result, it was chosen not to include the undamaged elastic moduli and the initial damage threshold in the vector of unknown variables to be calibrated. The performance of the DSID model was assessed after optimization, i.e., after transforming the constitutive equations to express them in terms of a_2 only. It is shown that within the set of assumptions made in this study, the DSID model indeed is not sensitive to C_0, except for higher values, above 10^6 Pa. In fact high damage thresholds delay the occurrence of damage under given stress conditions, so that only one constitutive parameter becomes insufficient to predict the stress/strain curves of damage claystone.

The advantage of the DSID model is that it provides a general mathematical framework to model the effects of crack-opening on stiffness and deformation, for complex stress including changes of principal directions, deviatoric stress in compression, and deviatoric stress in tension. The polynomials used in the expressions of the energy potentials are expressed in terms of independent invariants of stress and damage, and the formulation ensures thermodynamic consistency. The generality of the model is expected to allow its use for a wide range of brittle and quasi-brittle materials - rocks in particular. The number of damage parameters needed is rather limited (seven in total), but not straightforward to determine from laboratory tests. Probabilistic calibration and optimization promises to be an efficient tool that can be coupled to numerical codes in order to adapt the complexity of the DSID model to different rocks and stress paths. Further developments are currently on-going to calibrate, optimize and assess the DSID model for different types of rock, in order to highlight the potential need to enrich the continuum-based formulation of the DSID model with micro-structure de-

scriptors. Another study will focus on the performance of damage models when the stress path used for calibration does not match exactly the stress path undergone by the rock in the field.

References

[] H. Xu, C. Arson, Anisotropic Damage Models for Geomaterials: Theoretical and Numerical Challenges, International Journal of Computational Methods, Special Issue on Computational Geomechanics 11 (2).

[] J. Hemminger, G. Crabtree, M. Kastner, New Science for a Secure and Sustainable Energy Future, A Report from the Basic Energy Sciences Advisory Committee, U.S. Department of Energy, December 2008 .

[] P. Hughes, Geothermal (Ground-Source) Heat Pumps: Market Status, Barriers to Adoption, and Actions to Overcome Barriers, Oak Ridge National Laboratory, Report ORNL/TM-2008/232 .

[] H.-I. Wong, E. Desroches, L. Hansel, M.-H. Lagrange, H. Gourram, Trends of EDF's Fuel Core Management and Consequences on Fuel Cycle: "Cycle Impact" Analyses, in: Transactions - Fuel Cycles, Proceedings of the European Nuclear Conference (ENC 2012) - published on line in November 2012, Manchester, United Kingdom, 22–32, 2012.

[] BRC, Blue Ribbon Commission on America's Nuclear Future Draft Report to the Secretary of Energy, Tech. Rep., Blue Ribbon Commision, 2011.

[] E. Detournay, D. I. Garagash, The near-tip region of a fluid-driven fracture propagating in a permeable elastic solid, Journal of Fluid Mechanics 494 (2003) 1–32.

[] J. Adachi, E. Siebrits, A. Peirce, J. Desroches, Computer simulation of hydraulic fractures, International Journal of Rock Mechanics and Mining Sciences 44 (2007) 739–757.

[] P. Fu, S. M. Johnson, C. Carrigan, An explicitly coupled hydro-geomechanical model for simulating hydraulic fracturing in complex discrete fracture networks, International Journal for Numerical and Analytical Methods in Geomechanics online.

[] J. Zhao, Geothermal Testing and Measurements or Rock and Rock Fractures, Geothermics 23 (3) (1994) 215–231.

[] S.-Y. Yang, H.-D. Yeh, Modeling heat extraction from hot dry rock in a multi-well system, Applied Thermal Engineering 29 (8-9) (2009) 1676–1681.

[] H.-D. Yeh, S.-Y. Yang, K.-Y. Li, Heat extraction from aquifer geothermal systems, International Journal for Numerical and Analytical Methods in Geomechanics 36 (1) (2012) 85–99.

[] P. Bérest, J. Bergues, B. Brouard, J. Durup, B. Guerber, A salt cavern abandonment test, International Journal of Rock Mechanics and Mining Sciences 38 (3) (2001) 357–368.

[] S. Succar, R. H. Williams, Compressed air energy storage: Theory, resources, and applications for wind power, Princeton Environmental Institute Report 8.

[] H.-M. Kim, J. Rutqvist, D.-W. Ryu, B.-H. Choi, C. Sunwoo, W.-K. Song, Exploring the concept of compressed air energy storage (CAES) in lined rock caverns at shallow depth: a modeling study of air tightness and energy balance, Applied Energy 92 (2012) 653–667.

[] S. Kwon, J. Wilson, Deformation mechanism of the underground excavations at the WIPP site, Rock Mechanics and Rock Engineering 32 (2) (1999) 101–122.

[] J. Yow, J. Hunt, Coupled processes in rock mass performance with emphasis on nuclear waste isolation, International journal of rock mechanics and mining sciences 39 (2) (2002) 143–150.

[] R. Read, 20 years of excavation response studies at AECL's Underground Research Laboratory, International Journal of Rock Mechanics and Mining Sciences 41 (8) (2004) 1251–1275.

[] S. Olivella, A. Gens, Double structure THM analyses of a heating test in a fractured tuff incorporating intrinsic permeability variations, International Journal of Rock Mechanics and Mining Sciences 42 (5) (2005) 667–679.

[] S. Levasseur, R. Charlier, B. Frieg, F. Collin, Hydro-mechanical modelling of the excavation damaged zone around an underground excavation at Mont Terri Rock Laboratory, International Journal of Rock Mechanics and Mining Sciences 47 (3) (2010) 414–425.

[] L. Chiaramonte, M. Zoback, J. Friedmann, V. Stamp, Seal integrity and feasibility of CO2 sequestration in the Teapot Dome EOR pilot: geomechanical site characterization, Environmental Geology 54 (2008) 1667–1675.

[] H. Hassanzadeh, M. Pooladi-Darvish, D. Keith, Accelerating CO2 Dissolution in Saline Aquifers for Geological Storage s Mechanistic and Sensitivity Studies, Energy & Fuels 23 (2009) 3328–3336.

[] D. N. Espinoza, J. C. Santamarina, Water-CO2-mineral systems: Interfacial tension, contact angle, and diffusion - Implications to CO2 geological storage, Water Resources Research 46.

[] J. Rutqvist, The Geomechanics of CO2 Storage in Deep Sedimentary Formations, Geotechnical and Geological Engineering (2012) 1–27.

[] J. Lemaître, R. Desmorat, Engineering Damage Mechanics. Ductile, creep, fatigue and brittle failure., Springer - Verlag, Berlin Heidelberg, 2005.

[] J. Colovos, R. Brannon, P. Pinsky, Reduction of macroscale calibration experiments through constraints on anisotropic elastic stiffnesses, the 47th US Rock Mechanics/Geomechancis Symposium, San Francisco, California, 2013.

[] A. Ledesma, A. Gens, E. Alonso, Estimation of parameters in geotechnical backanalysis—I. Maximum likelihood approach, Computers and Geotechnics 18 (1) (1996) 1–27.

[] B.-C. Jung, G. Biscontin, P. Gardoni, Bayesian updating of a unified soil compression model, Georisk 3 (2) (2009) 87–96.

[] B.-C. Jung, P. Gardoni, G. Biscontin, Probabilistic soil identification based on cone penetration tests, Geotechnique 58 (7) (2008) 591–603.

[] Z. Medina-Cetina, C. Arson, Probabilistic Calibration of a Damage Rock Mechanics Model, Géotechnique Letters (2014) (in press).

[] C. Arson, Z. Medina-Cetina, Bayesian Paradigm to Assess Rock Compression Damage Models, Environmental Geotechnics (2014) (in press).

[] L. Boyce, C. Chamis, Probabilistic constitutive relationships for cyclic material strength models, Journal of Propulsion and Power 8 (1) (1992) 227–232.

[] P. Gardoni, R. G. Pillai, M. B. D. Hueste, K. Reinschmidt, D. Trejo, Probabilistic capacity models for corroding posttensioning strands calibrated using laboratory results, Journal of engineering mechanics 135 (9) (2009) 906–916.

[] P. Gardoni, D. Trejo, M. Vannucci, C. Bhattacharjee, Probabilistic models for modulus of elasticity of self-consolidated concrete: bayesian approach, Journal of engineering mechanics 135 (4) (2009) 295–306.

[] T. Tsuchiya, O. Tabata, J. Sakata, Y. Taga, Specimen size effect on tensile strength of surface-micromachined polycrystalline silicon thin films, Microelectromechanical Systems, Journal of 7 (1) (1998) 106–113.

[] Q. Huang, P. Gardoni, S. Hurlebaus, Predicting Concrete Compressive Strength Using Ultrasonic Pulse Velocity and Rebound Number, ACI Materials Journal 108 (4) (2011) 403–412.

[] D. Trejo, R. G. Pillai, M. B. D. Hueste, K. F. Reinschmidt, P. Gardoni, Parameters influencing corrosion and tension capacity of post-tensioning strands, ACI Materials Journal 106 (2).

[] R. G. Pillai, P. Gardoni, D. Trejo, M. B. D. Hueste, K. F. Reinschmidt, Probabilistic Models for the Tensile Strength of Corroding Strands in Posttensioned Segmental Concrete Bridges, Journal of Materials in Civil Engineering 22 (10) (2010) 967–977.

[] F. Z. ans S.Y. Xie, D. Hu, J. Shao, B. Gatmiri, Effect of water content and structural anisotropy on mechanical property of claystone, Applied Clay Science 69 (2012) 79–86.

[] A. Chiarelli, J. Shao, H. Hoteit, Modeling of elastoplastic damage behavior of a claystone, International Journal of Plasticity 19 (2003) 23–45.

[] M. Souley, G. Armand, K. Su, M. Ghoreychi, Modeling the viscoplastic and damage behavior in deep argillaceous rocks, Physics and Chemistry of the Earth 36 (2011) 1949–1959.

[] F. Bourgeois, J. Shao, O. Ozanam, An elastoplastic model for unsaturated rocks and concrete, Mechanics Research Communications 29 (2002) 383–390.

[] J. F. Shao, G. Duveau, F. Bourgeois, , W. Z. Chen, Elastoplastic Damage Modeling in Unsaturated Rocks and Applications, International Journal of Geomechanics 6 (2006) 119–130.

[] Y. Jia, X. Song, G. Duveau, K. Su, J. Shao, Elastoplastic damage modelling of argillite in partially saturated condition and application, Physics and Chemistry of the Earth (32) (2007) 656–666.

[] Y. Jia, H. Bian, G. Duveau, K. Su, J. Shao, Hydromechanical modelling of shaft excavation in Meuse/Haute-Marne laboratory, Physics and Chemistry of the Earth 33 (2008) S422–S435.

[] Y. Jia, H. Bian, G. Duveau, K. Su, J. Shao, Numerical modelling of in situ behaviour of the Callovo–Oxfordian argillite subjected to the thermal loading, Engineering Geology 109 (2009) 262–272.

[] W. Shen, J. Shao, D. Kondo, B. Gatmiri, A micro–macro model for clayey rocks with a plastic compressible porous matrix, International Journal of Plasticity 36 (2012) 64–85.

[] W. Shen, D. Kondo, L. Dormieux, J. Shao, A closed-form three scale model for ductile rocks with a plastically compressible porous matrix, Mechanics of Materials 59 (2013) 73–86.

[] C. Arson, B. Gatmiri, On damage modelling in unsaturated clay rocks, Physics and Chemistry of the Earth 33 (2008) S407–S415.

[] C. Arson, B. Gatmiri, A mixed damage model for unsaturated porous media, Comptes-Rendus de l'Académie des Sciences de Paris, section Mécanique 337 (2009) 68–74.

[] C. Arson, B. Gatmiri, Thermo-Hydro-Mechanical Modeling of Damage in Unsaturated Porous Media: Theoretical Framework and Numerical Study of the EDZ, International Journal for Numerical and Analytical Methods in Geomechanics 36 (2012) 272–306.

[] C. Zhu, C. Arson, A Thermo-Mechanical Damage Model for Rock Stiffness during Anisotropic Crack Opening and Closure, Acta Geotechnica (2014) DOI: 10.1007/s11440–013–0281–0 (in press).

[] C. Arson, H. Xu, F. Chester, On The Definition Of Damage In Time-Dependent Healing Models For Salt Rock, Géotechnique Letters (2012) DOI: 10.1680/geolett.12.00013.

[] D. Halm, A. Dragon, An anisotropic model of damage and frictional sliding for brittle materials, Eur. J. Mech. A/ Solids 17 (3) (1998) 439–460.

[] D. Halm, A. Dragon, Modelisation de l'endommagement par mesofissuration du granite, Revue Francaise de Genie Civi. 17 (2002) 21–33.

[] R. K. Abu Al-Rub, S.-M. Kim, Computational applications of a coupled plasticity-damage constitutive model for simulating plain concrete fracture., Engineering Fracture Mechanics 77 (2010) 1577–1603.

[] U. Cicekli, G. Z. Voyiadjis, R. K. Abu Al-Rub, A plasticity and anisotropic damage model for plain concrete., International Journal of Plasticity 23 (2007) 1874–1900.

[] S. Murakami, K. Kamiya, Constitutive and damage evolution equations of elastic-brittle materials based on irreversible thermodynamics, Int. J. Mech. Sci. 39 (1996) 473–486.

[] F. Homand-Etienne, D. Hoxha, J. F. Shao, A Continuum Damage Constitutive Law for Brittle Rocks, Computers and Geotechnics 22 (2) (1998) 135–151.

[] J.-L. Chaboche, Development of continuum damage mechanics for elastic solids sustaining anisotropic and unilateral damage, International Journal of Damage Mechanics 2 (1993) 311–329.

[] F. Pellet, A. Hajdu, F. Deleruyelle, F. Besnus, A viscoplastic model including anisotropic damage for the time dependent behaviour of rock, Int. J. Numer. Anal. Meth. Geomech. 29 (2005) 941–970.

[] M. Ortiz, A constitutive theory for the inelastic behaviour of concrete, Mech. Mater. 4 (1985) 67–93.

[] J. Shao, H. Zhou, K. Chau, Coupling between anisotropic damage and permeability variation in brittle rocks., International Journal for Numerical and Analytical Methods in Geomechanics 29 (12) (2005) 1231–1247.

[] K. Hayakawa, S. Murakami, Thermodynamical modeling of elastic-plastic damage and experimental validation of damage potential, International Journal of Damage Mechanics 6 (1997) 333–363.

[] J. F. Shao, J. W. Rudnicki, A microcrack-based continuous damage model for brittle geomaterials, Mechanics of Materials 32 (2000) 607–619.

[] Y. F. Lu, J. F. Shao, Modelling of anisotropic damage in brittle rocks under compression dominated stresses, International Journal for Numerical and Analytical Methods in Geomechanics 26 (2002) 945–961.

[] G. T. Houlsby, A. M. Puzrin, Principles of hyperplasticity an approach to plasticity theory based on thermodynamic principles, Springer, London, 2006.

[] H. S. Yu, Plasticity and Geotechnics, Springer, New York, N.Y., 2006.

[] G. E. Box, D. R. Cox, An analysis of transformations, Journal of the Royal Statistical Society. Series B (Methodological) (1964) 211–252.

[] P. Gardoni, A. Der Kiureghian, K. M. Mosalam, Probabilistic capacity models and fragility estimates for reinforced concrete columns based on experimental observations, Journal of Engineering Mechanics 128 (10) (2002) 1024–1038.

[] D. C. Montgomery, G. C. Runger, Applied statistics and probability for engineers, Wiley. com, 2010.

[] A. Gelman, J. B. Carlin, H. S. Stern, D. B. Rubin, Bayesian data analysis, CRC press, 2003.

[] G. E. Box, G. C. Tiao, Bayesian inference in statistical analysis, vol. 40, John Wiley & Sons, 2011.

[] J. F. Shao, Y. F. Lu, , D. Lydzba, Damage Modeling of Saturated Rocks in Drained Damage Modeling of Saturated Rocks in Drained and Undrained Conditions, Journal of Engineering Mechanics 130 (6) (2004) 733–740.

[] C. J. Stone, A course in probability and statistics, Duxbury Press Belmont:, 1996.

Table 1: Summary of the Mineral and Physical Characterisitcs of Claystone.

Origin	Physical Properties						
	Minerals	Density	Porosity	Permeability	Water Content	Saturation	Grain Size
Meuse/Haute Marne (Paris Basin)	Calcite: $27 \pm 9\%$; Quartz: $23 \pm 4\%$; Clay matrix: $45 \pm 7\%$. Some accessory minerals are subordinate feldspars, pyrite, and iron oxides, about a volumetric fraction of 5%. The clay mineral composition is relatively constant at 65% I/S (illite/smectite interstratified minerals), 30% illite and 5% kaolinite and chlorite.	The bulk, dry and grain density are respectively 2.41 ± 0.06, 2.27 ± 0.03 and 2.65 g/cm^3	$11.8 \pm 1.6\%$	$10^{-19} - 10^{-20}$m^2	$6.2 \pm 1.38\%$	$95 \pm 1.1\%$	the average size of calcite and quartz grains is generally less than 200 μm.
[?] Eastern France	Quartz: 52%; Calcite: about 28%; Clays (smectite, illite, kaolinite and chlorite).			intrinsic permeability 10^{-20}m^2			
	Calcite: $20 - 40\%$, Quartz $20 - 30\%$, clays $40 - 55\%$		$11.5 - 12\%$		$4 - 5.7\%$		
	Calcite: $25 - 55\%$, Quartz $20 - 30\%$, clays $35 - 55\%$		$11 - 13.5\%$		$4 - 7\%$		
	Calcite: $25 - 35\%$, Quartz $15 - 20\%$, clays $45 - 60\%$		12%		$4 - 7\%$		
[?] Eastern France				intrinsic permeability 10^{-21}m^2			
				intrinsic permeability $k = 10^{-21}$m$^2, \mu = 10^{-3}$ Pa s			

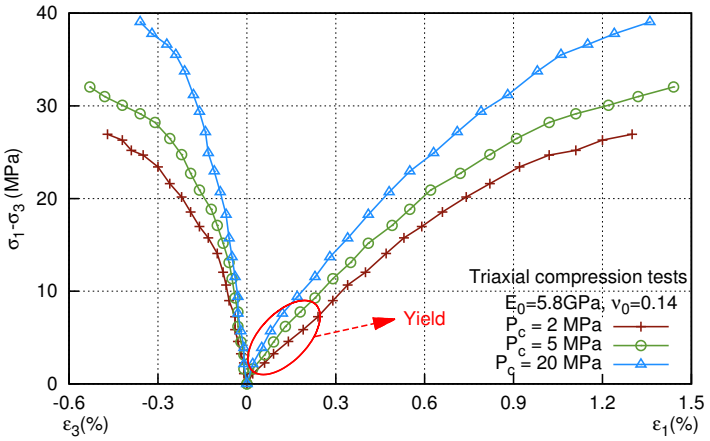

Figure 1: Typical stress/strain curves of claystone during triaxial compression tests (re-plotted, after [**?**]): effect of the confining pressure (p_c) on the initiation of damage and on damage-induced anisotropy.

Table 2: Thermodynamic framework of the DSID model.

	D.S.I.D. Model
1. Free Energy	$G_s(\boldsymbol{\sigma},\boldsymbol{\Omega}) = \frac{1}{2}\boldsymbol{\sigma} : \mathbb{S}_0 : \boldsymbol{\sigma} + a_1\,\mathrm{Tr}\boldsymbol{\Omega}(\mathrm{Tr}\boldsymbol{\sigma})^2 + a_2\,\mathrm{Tr}(\boldsymbol{\sigma}\cdot\boldsymbol{\sigma}\cdot\boldsymbol{\Omega}) + a_3\,\mathrm{Tr}\boldsymbol{\sigma}\,\mathrm{Tr}(\boldsymbol{\Omega}\cdot\boldsymbol{\sigma}) + a_4\,\mathrm{Tr}\boldsymbol{\Omega}\,\mathrm{Tr}(\boldsymbol{\sigma}\cdot\boldsymbol{\sigma})$
	$\boldsymbol{\epsilon}^E = \frac{\partial G_s}{\partial \boldsymbol{\sigma}} = \frac{1+\nu_0}{E_0}\boldsymbol{\sigma} - \frac{\nu_0}{E_0}(\mathrm{Tr}\boldsymbol{\sigma})\,\boldsymbol{\delta} + 2a_1(\mathrm{Tr}\boldsymbol{\Omega}\,\mathrm{Tr}\boldsymbol{\sigma})\,\boldsymbol{\delta} + a_2(\boldsymbol{\sigma}\cdot\boldsymbol{\Omega}+\boldsymbol{\Omega}\cdot\boldsymbol{\sigma}) + a_3[\,\mathrm{Tr}(\boldsymbol{\sigma}\cdot\boldsymbol{\Omega})\,\boldsymbol{\delta} + (\mathrm{Tr}\boldsymbol{\sigma})\,\boldsymbol{\Omega}\,] + 2a_4(\mathrm{Tr}\boldsymbol{\Omega})\,\boldsymbol{\sigma}$
	$\mathbf{Y} = \frac{\partial G_s}{\partial \boldsymbol{\Omega}} = a_1(\mathrm{Tr}\boldsymbol{\sigma})^2\,\boldsymbol{\delta} + a_2\boldsymbol{\sigma}\cdot\boldsymbol{\sigma} + a_3\mathrm{Tr}(\boldsymbol{\sigma})\boldsymbol{\sigma} + a_4\mathrm{Tr}(\boldsymbol{\sigma}\cdot\boldsymbol{\sigma})\boldsymbol{\delta}$
2. Damage Function	$f_d = \sqrt{J^*} - \alpha I^* - k$
	$J^* = \frac{1}{2}(\mathbb{P}_1 : \mathbf{Y} - \frac{1}{3}I^*\boldsymbol{\delta}) : (\mathbb{P}_1 : \mathbf{Y} - \frac{1}{3}I^*\boldsymbol{\delta}), \quad I^* = (\mathbb{P}_1 : \mathbf{Y}) : \boldsymbol{\delta}$
	$\mathbb{P}_1(\boldsymbol{\sigma}) = \sum_{p=1}^{3}\left[H(\sigma^{(p)}) - H(-\sigma^{(p)})\right]\mathbf{n}^{(p)}\otimes\mathbf{n}^{(p)}\otimes\mathbf{n}^{(p)}\otimes\mathbf{n}^{(p)}$
	$k = C_0 - C_1\mathrm{Tr}(\boldsymbol{\Omega})$
3. Damage Potential	$g_d = \sqrt{\frac{1}{2}(\mathbb{P}_2 : \mathbf{Y}) : (\mathbb{P}_2 : \mathbf{Y})}$
	$\mathbb{P}_2 = \sum_{p=1}^{3} H\left[\max_{q=1}^{3}(\sigma^{(q)}) - \sigma^{(p)}\right]\,\mathbf{n}^{(p)}\otimes\mathbf{n}^{(p)}\otimes\mathbf{n}^{(p)}\otimes\mathbf{n}^{(p)}$
4. Flow Rules	$\boldsymbol{\epsilon} = \boldsymbol{\epsilon}^E + \boldsymbol{\epsilon}^{id}, \qquad \dot{\boldsymbol{\epsilon}}^{id} = \dot{\lambda}_d\frac{\partial f_d}{\partial \boldsymbol{\sigma}} = \dot{\lambda}_d\frac{\partial f_d}{\partial \mathbf{Y}} : \frac{\partial \mathbf{Y}}{\partial \boldsymbol{\sigma}}$
	$\dot{\boldsymbol{\Omega}} = \dot{\lambda}_d\frac{\partial g_d}{\partial \mathbf{Y}}$

G_s: Gibbs free energy	$\boldsymbol{\sigma}$: Stress tensor	$\boldsymbol{\Omega}$: Damage variable
$\boldsymbol{\epsilon}^E$: Cumul. elastic strain	ν_0: Poisson's ratio	$\mathbb{S}_0$: Undamaged compliance tensor
E_0: Young's Modulus	$\boldsymbol{\delta}$: Kronecker delta	$\mathbf{Y}$: Damage driving force
f_d: Damage function	$H(\cdot)$: Heaviside function	$\mathbb{P}_1$ and $\mathbb{P}_2$: Projection tensors
g_d: Damage potential	C_0: Initial damage threshold	$\max(\cdot)$: Maximum function
$\dot{\lambda}_d$: Lagrangian Multiplier	$\dot{\boldsymbol{\epsilon}}^{id}$: Irreversible strain rate	$\dot{\boldsymbol{\Omega}}$: Damage rate
a_1, a_2, a_3, a_4: Material parameters	$\sigma^{(p)}$ and $\mathbf{n}^{(p)}$: p^{th} principal stress, p^{th} principal vector	C_1: Damage hardening variable

Table 3: Experimental results used as reference datasets in the probabilistic calibration.

References	Elastic parameters		
	Number of tests	E_0	ν_0
Chiarelli *et al.*, 2003 [**?**]	12	7.6GPa	0.14
Bourgeois *et al.*, 2002 [**?**]	3	5.8GPa	0.14
Souley *et al.*, 2011 [**?**]	1	4GPa	0.3

Table 4: Initial set of damage parameters for probabilistic calibration (from [**?** **?**]).

a_1 (Pa^{-1})	a_2 (Pa^{-1})	a_3 (Pa^{-1})	a_4 (Pa^{-1})	C_0 (Pa)	C_1 (Pa)	α (-)
1.26E-13	3.94E-11	-1.26E-12	2.51E-13	1.10E+5	2.20E+6	2.31E-1

Table 5: Damage parameters calibrated with the maximum likelihood method, with $C_0 = 1.1 \times 10^5$ Pa.

param.	μ	scale	SD	C.O.V
a_1 (Pa^{-1})	21.92	10^{-13}	1.28	0.06
a_2 (Pa^{-1})	704.94	10^{-11}	28.58	0.04
a_3 (Pa^{-1})	-98.88	10^{-12}	5.15	0.05
a_4 (Pa^{-1})	11.10	10^{-13}	1.04	0.09
C_1 (Pa)	64.35	10^6	4.02	0.06
α (-)	3.31	0.1	0.09	0.03
s	0.2875	1	-	-

μ: mean value. SD: standard deviation. C.O.V.: coefficient Of Variation.

Table 6: Damage parameters calibrated with the maximum likelihood method, with $C_0 = 1.1 \times 10^5$ Pa, after removing a_4.

param.	μ	scale	SD	C.O.V
a_1 (Pa^{-1})	21.92	10^{-13}	1.00	0.05
a_2 (Pa^{-1})	704.94	10^{-11}	13.02	0.02
a_3 (Pa^{-1})	-98.88	10^{-12}	3.80	0.04
C_1 (Pa)	64.35	10^6	1.35	0.02
α (-)	3.30	0.1	0.05	0.02
s	0.2881	1	-	-

μ: mean value. SD: standard deviation. C.O.V.: coefficient Of Variation.

Table 7: Damage parameters calibrated with the maximum likelihood method, with $C_0 = 1.1 \times 10^5$ Pa, after removing a_4 and a_1.

param.	μ	scale	SD	C.O.V
a_2 (Pa^{-1})	704.94	10^{-11}	31.1	0.04
a_3 (Pa^{-1})	-98.88	10^{-12}	5.9	0.06
C_1 (Pa)	64.35	10^6	1.00	0.02
α (-)	3.31	0.1	0.07	0.02
s	0.3011	1	-	-

μ: mean value. SD: standard deviation. C.O.V.: coefficient Of Variation.

Table 8: Damage parameters calibrated with the maximum likelihood method, with $C_0 = 1.1 \times 10^5$ Pa, after removing a_4, a_1 and a_3.

param.	μ	scale	SD	C.O.V
a_2 (Pa^{-1})	704.94	10^{-11}	35.80	0.05
C_1 (Pa)	64.34	10^6	6.30	0.10
α (-)	3.29	0.1	0.26	0.08
s	0.2862	1	-	-

μ: mean value. SD: standard deviation. C.O.V.: coefficient Of Variation.

Table 9: Correlation coefficient matrix for the DSID model parameters, using only a_2.

param.	a_2 (Pa^{-1})	C_1 (Pa)	α (-)
a_2 (Pa^{-1})	1	1	0.99
C_1 (Pa)	1	1	0.99
α (-)	0.99	0.99	1

Table 10: Optimized DSID parameters, calibrated with the maximum likelihood method, using a_2 as the sole constitutive parameter.

param.	Suggested Value	SD
a_2 (Pa^{-1})	704.94×10^{-11}	35.80×10^{-11}
$\hat{C}_1$ (Pa)	$64.34 \times 10^6 + 1.76 \times 10^{17} \left(a_2 - 704.94 \times 10^{-11}\right)$	6.30×10^6
$\hat{\alpha}$ (-)	$3.29 \times 10^{-1} + 7.26 \times 10^9 \left(a_2 - 704.94 \times 10^{-11}\right)$	0.026×10^{-1}
s	0.2862	-

SD: standard deviation

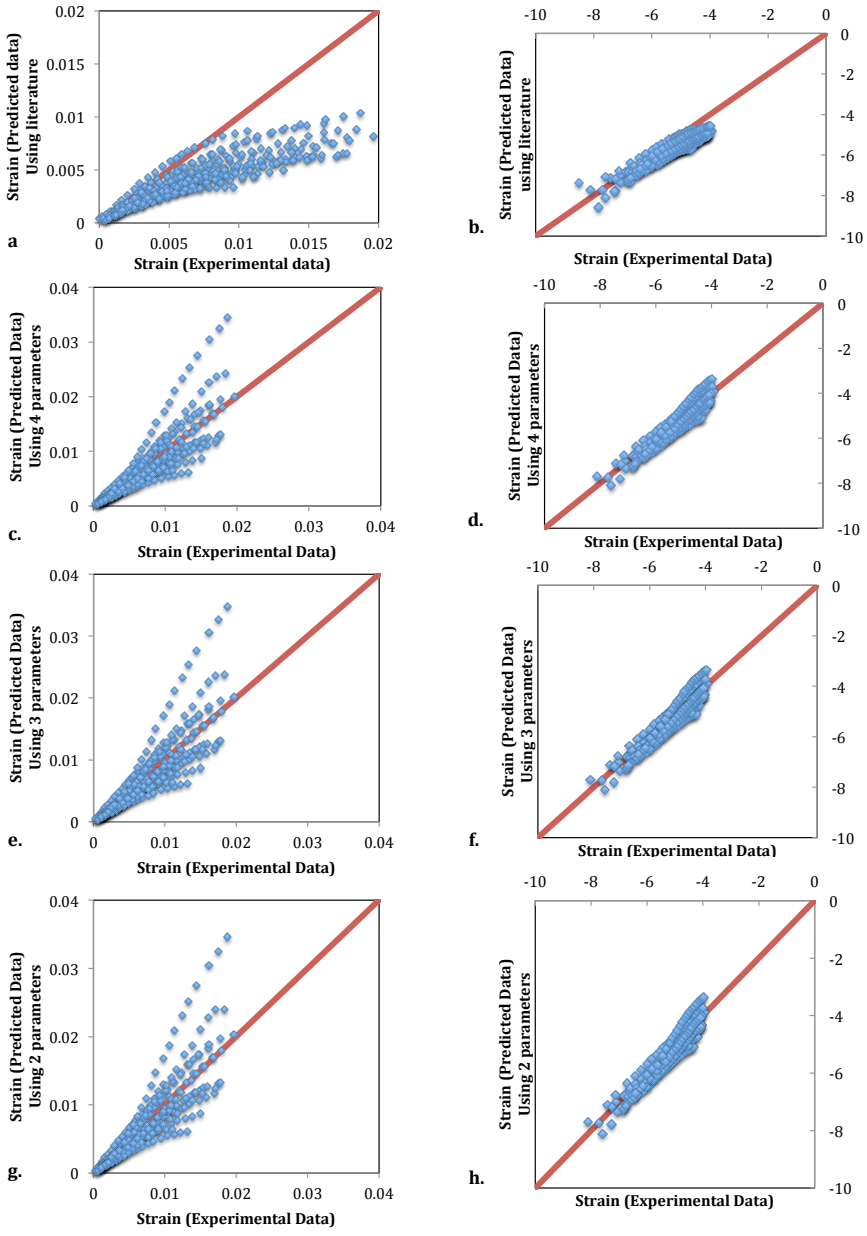

Figure 2: Comparison of the deformation predicted with the DSID model with deformation points taken from experimental stress/strain curves reported in Table **??**. Plots on the left (resp. on the right) display the results before (resp. after) performing the logarithmic transformation of strain. (a)&(b): Before model calibration, using model parameters obtained by curve-fitting in [**?** **?**]. (c)&(d): After calibration based on the Maximum Likelihood Method. (e)&(f): After calibration, without a_4. (g)&(h): After calibration, without a_4 and a_1.

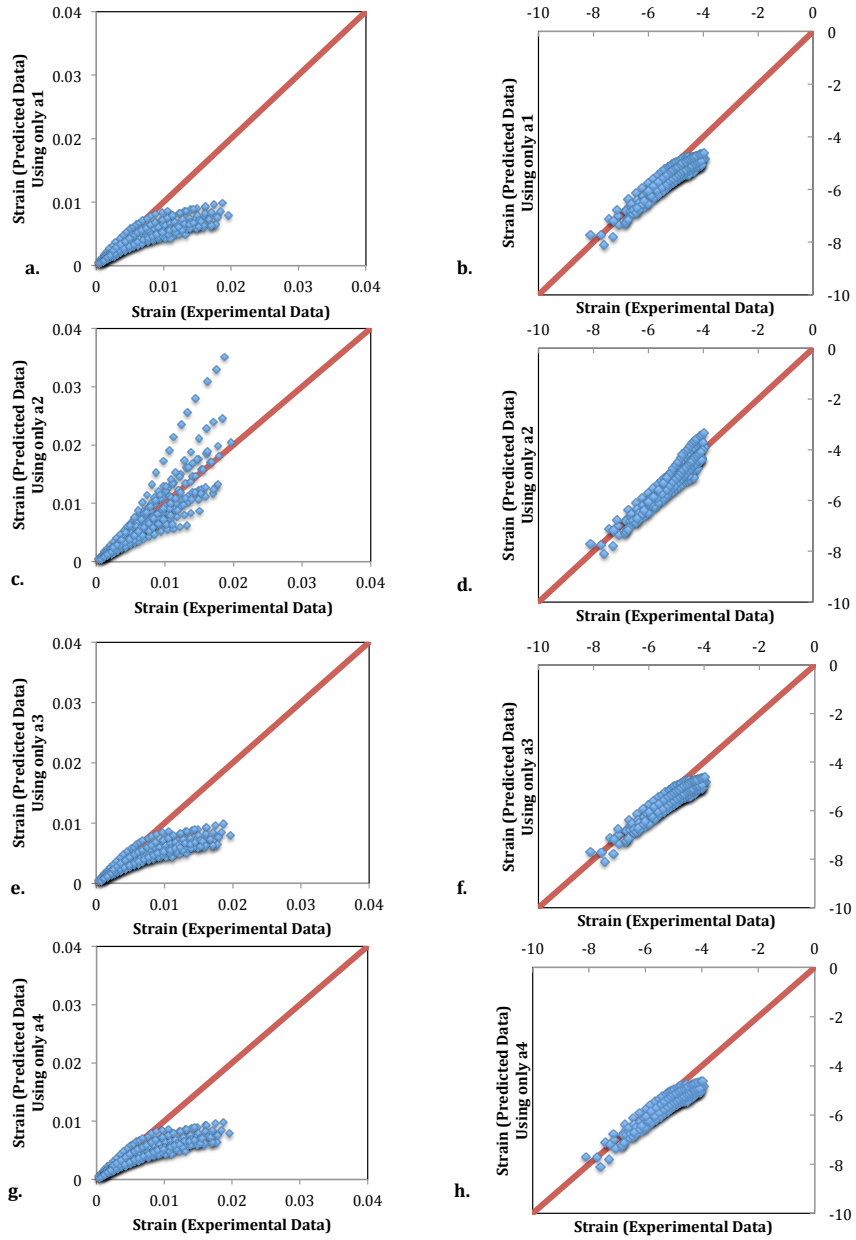

Figure 3: Performance of the DSID model to predict experimental stress/strain curves reported in Table **??**, when only one constitutive model parameter is used in the formulation. Plots on the left (resp. on the right) display the results before (resp. after) performing the logarithmic transformation of strain. (a)&(b): Only a_1. (c)&(d): Only a_2. (e)&(f): Only a_3. (g)&(h): Only a_4.

Table 11: Relative influence of the a_i parameters in the formulation of the DSID model.

a_i	μ	Scale	Terms in G_s	Terms in $\boldsymbol{\epsilon}^E$	Terms in $\mathbf{Y}$	Reduction
a_1	21.92	10^{-13}	$\mathrm{Tr}\boldsymbol{\Omega}(\mathrm{Tr}\boldsymbol{\sigma})^2$	$(\mathrm{Tr}\boldsymbol{\Omega}\,\mathrm{Tr}\boldsymbol{\sigma})\boldsymbol{\delta}$	$(\mathrm{Tr}\boldsymbol{\sigma})^2\boldsymbol{\delta}$	2
a_2	704.94	10^{-11}	$\mathrm{Tr}(\boldsymbol{\sigma}\cdot\boldsymbol{\sigma}\cdot\boldsymbol{\Omega})$	$(\sigma\cdot\boldsymbol{\Omega}+\boldsymbol{\Omega}\cdot\boldsymbol{\sigma})$	$\boldsymbol{\sigma}\cdot\boldsymbol{\sigma}$	-
a_3	-98.88	10^{-12}	$\mathrm{Tr}\boldsymbol{\sigma}\,\mathrm{Tr}(\boldsymbol{\Omega}\cdot\boldsymbol{\sigma})$	$\mathrm{Tr}(\boldsymbol{\sigma}\cdot\boldsymbol{\Omega})\boldsymbol{\delta}+(\mathrm{Tr}\boldsymbol{\sigma}\boldsymbol{\Omega})$	$\mathrm{Tr}(\boldsymbol{\sigma})\boldsymbol{\sigma}$	3
a_4	11.10	10^{-13}	$\mathrm{Tr}\boldsymbol{\Omega}\,\mathrm{Tr}(\boldsymbol{\sigma}\cdot\boldsymbol{\sigma})$	$(\mathrm{Tr}\boldsymbol{\Omega})\boldsymbol{\sigma}$	$\mathrm{Tr}(\boldsymbol{\sigma}\cdot\boldsymbol{\sigma})\boldsymbol{\delta}$	1

The "reduction" column indicates in which order the model parameters should be removed, according to their relative importance in the DSID model formulation.

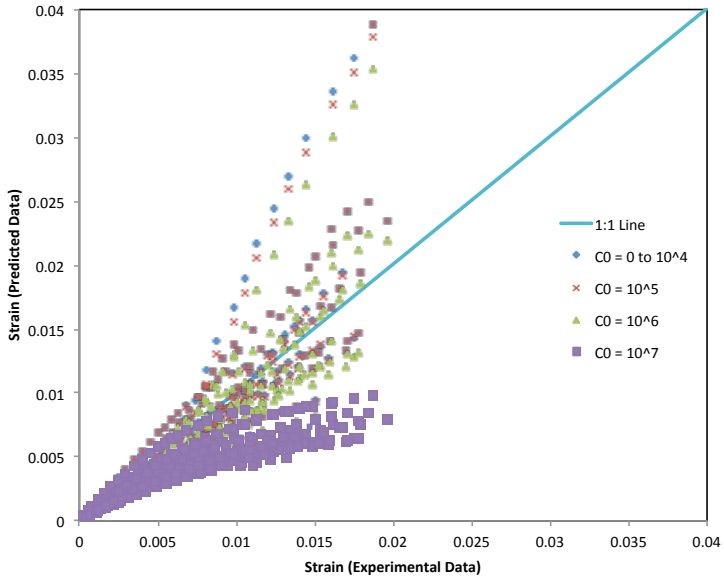

Figure 4: Performance of the DSID model to predict stress/strain curves during triaxial compression and proportional tests, using a_2 (in Pa^{-1}) as the sole constitutive parameter, with various values for the initial damage threshold C_0 (in Pa).

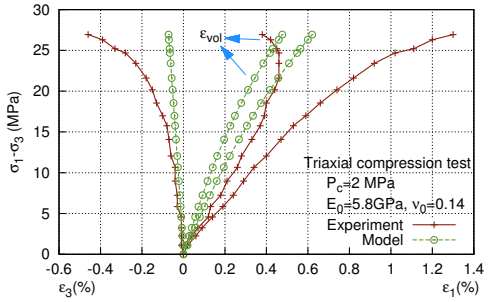

(a) Test 1 (Experimental data from [**?**])

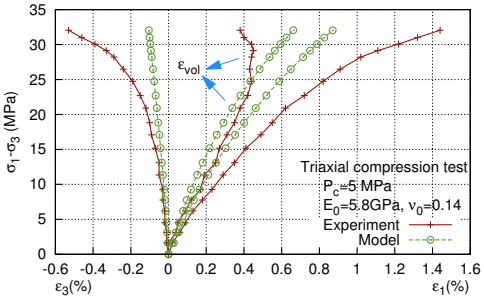

(b) Test 2 (Experimental data from [**?**])

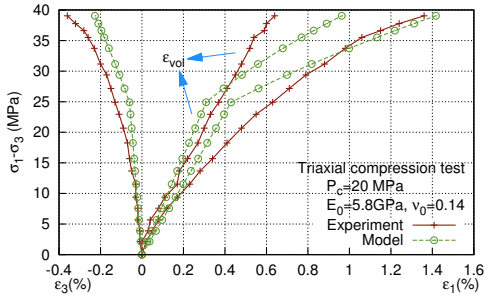

(c) Test 3 (Experimental data from [**?**])

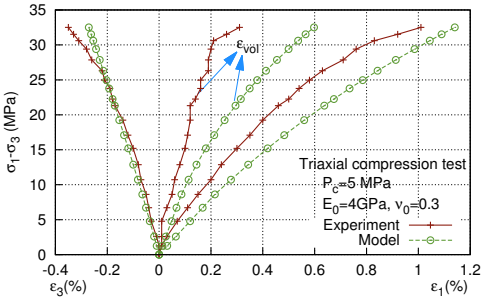

(d) Test 4 (Experimental data from [**?**])

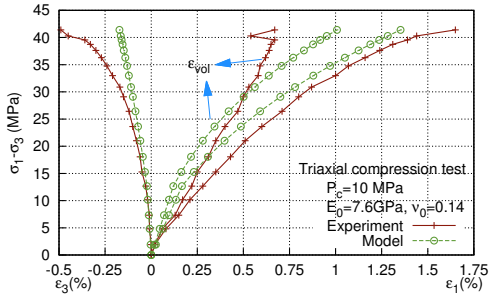

(e) Test 5 (Experimental data from [**?**])

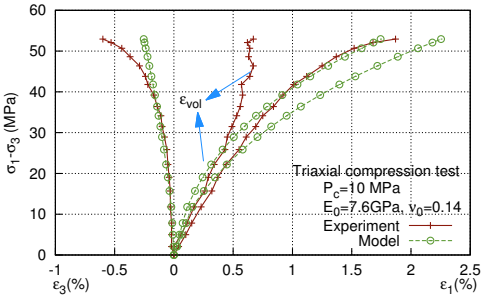

(f) Test 6 (Experimental data from [**?**])

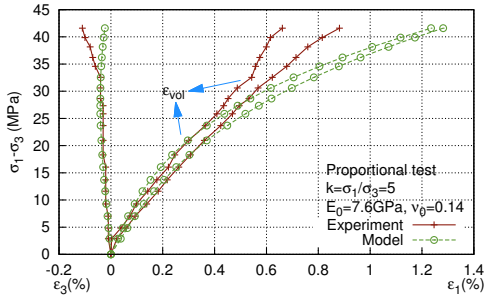

(g) Test 7 (Experimental data from [**?**])

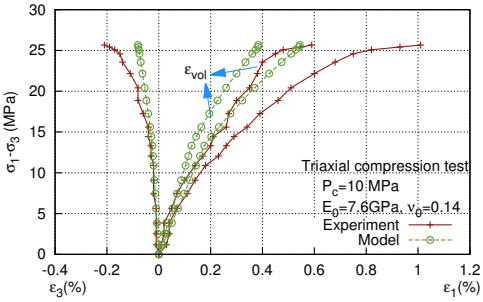

(h) Test 8 (Experimental data from [**?**])

Figure 5: Comparison between model predictions and experimental data, after model optimization: stress/strain plots for tests 1–8

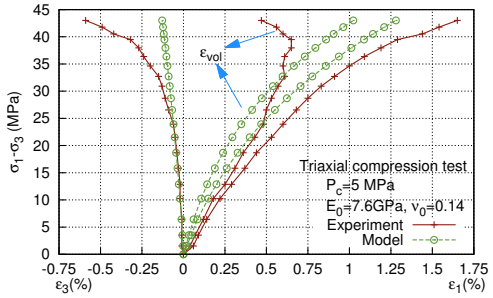

(a) Test 9 (Experimental data from [**?**])

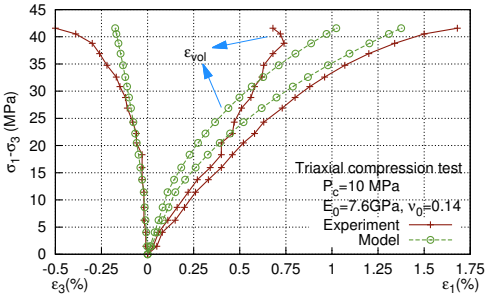

(b) Test 10 (Experimental data from [**?**])

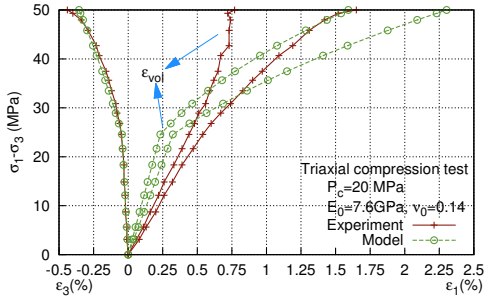

(c) Test 11 (Experimental data from [**?**])

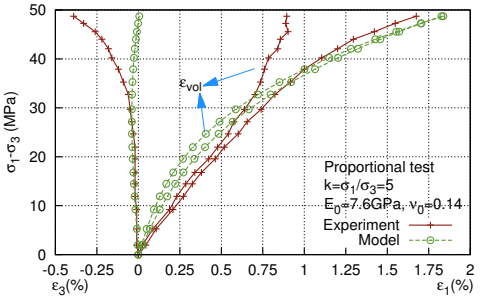

(d) Test 12 (Experimental data from [**?**])

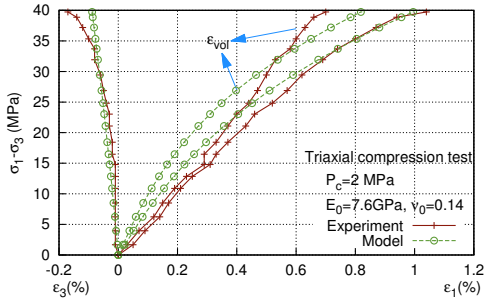

(e) Test 13 (Experimental data from [**?**])

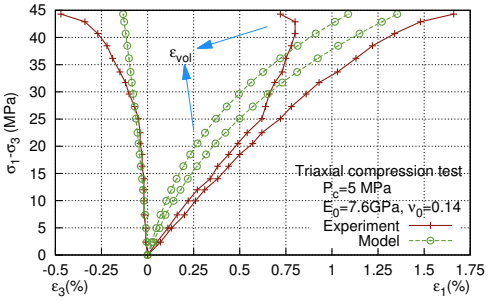

(f) Test 14 (Experimental data from [**?**])

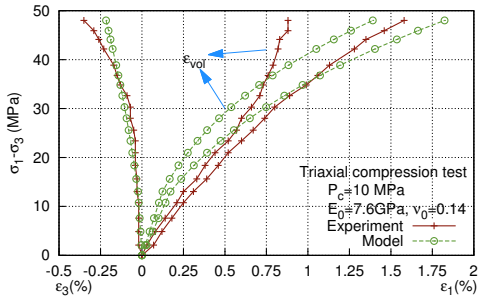

(g) Test 15 (Experimental data from [**?**])

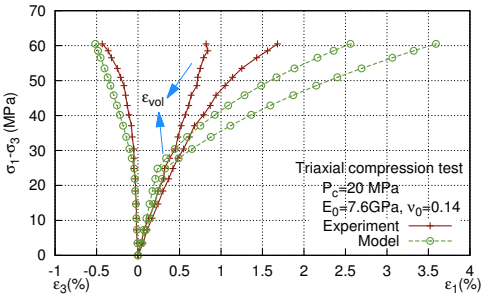

(h) Test 16 (Experimental data from [**?**])

Figure 6: Comparison between model predictions and experimental data, after model optimization: stress/strain plots for tests 9–16